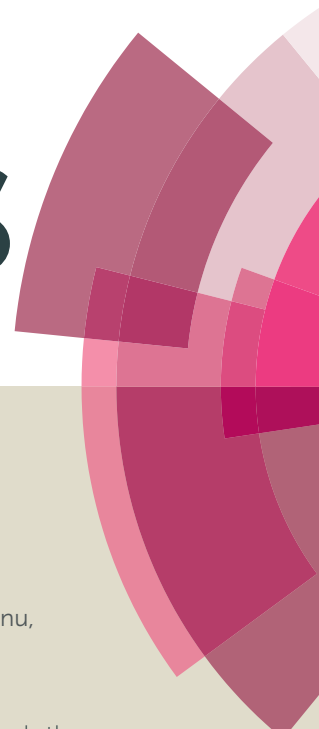


# RSC Advances



This article can be cited before page numbers have been issued, to do this please use: M. D. Damaceanu, M. Mihaila, C. Constantin, S. Chisca, B. Serban, C. Diaconu, O. Buiu, E. M. Pavelescu and M. Kusko, *RSC Adv.*, 2015, DOI: 10.1039/C5RA07939J.



This is an *Accepted Manuscript*, which has been through the Royal Society of Chemistry peer review process and has been accepted for publication.

*Accepted Manuscripts* are published online shortly after acceptance, before technical editing, formatting and proof reading. Using this free service, authors can make their results available to the community, in citable form, before we publish the edited article. This *Accepted Manuscript* will be replaced by the edited, formatted and paginated article as soon as this is available.

You can find more information about *Accepted Manuscripts* in the [Information for Authors](#).

Please note that technical editing may introduce minor changes to the text and/or graphics, which may alter content. The journal's standard [Terms & Conditions](#) and the [Ethical guidelines](#) still apply. In no event shall the Royal Society of Chemistry be held responsible for any errors or omissions in this *Accepted Manuscript* or any consequences arising from the use of any information it contains.



Journal Name

ARTICLE

## A new sensitizer containing dihexyloxy-substituted triphenylamine as donor and a binary conjugated spacer for dye-sensitized solar cells

Received 00th January 20xx,  
Accepted 00th January 20xx

DOI: 10.1039/x0xx00000x

www.rsc.org/

Mariana-Dana Damaceanu<sup>a\*</sup>, Mihai Mihaila<sup>b,c</sup>, Catalin-Paul Constantin<sup>a</sup>, Stefan Chisca<sup>a</sup>, Bogdan-Catalin Serban<sup>b</sup>, Cristian Diaconu<sup>b</sup>, Octavian Buiu<sup>b</sup>, Emil Mihai Pavelescu<sup>c</sup>, Mihaela Kusko<sup>c</sup>

The synthesis and application to dye-sensitized solar cells (DSSC) of a new dihexyloxy-substituted triphenylamine-based organic dye is reported. The dye design, based on the push-pull concept, consists of dihexyloxy-substituted triphenylamine as an electron donor and a cyanoacrylic acid as an anchoring and electron acceptor connected through a  $\pi$ -conjugated bridge. The electron spacer containing furan and thiophene moieties were employed in the dye sensitizer for expansion of the  $\pi$ -conjugated fragment as to adjust the absorption spectra and HOMO/LUMO levels of the dye. The relationship between the dye chemical structure and the photophysical, electrochemical, and photovoltaic properties by spectral, electrochemical, photovoltaic experiments, and density functional theory calculations was thoroughly investigated. The photovoltaic performance of the dye as sensitizer was assessed in DSSC cells realized using electrolytes containing the iodide/triiodide redox couple. The cells obtained with the new dye show a power conversion efficiency of 5.14 %, without using any coadsorbant and optimization.

### 1. Introduction

In response to energy demands and environment pollution, intensive efforts have been carried out to find and develop sustainable energy solutions. Solar energy is one of the fastest growing renewable energy sources: it does not produce pollutants or harmful byproducts and is free of emissions. Organic solar cells emerged as highly promising and cost-effective alternative for the photovoltaic energy sector<sup>1</sup>. Among them, dye-sensitized solar cells (DSSCs) have received considerable attention due to their high performances and low cost of production<sup>2</sup>. An important feature of the DSSC is the dye anchored on the TiO<sub>2</sub> surface, which act as light absorber. Several metal-organic complexes have been widely investigated as sensitizers of DSSCs. Among them, ruthenium-based sensitizers exhibit the highest validated power conversion efficiency<sup>3-5</sup>.

Metal - free organic chromophores are considered as a viable alternative to ruthenium dyes in DSSCs due to their well-known advantages: high molar extinction coefficients, versatile and relatively cheap synthesis (i.e., no noble metal is involved),

attainable structural tuning and less environmental issues<sup>6-8</sup>. Many of these structures are of push-pull type featuring a donor (D) and acceptor (A) segments connected through a  $\pi$ -conjugated bridge (D- $\pi$ -A). Indoline<sup>9</sup>, triphenylamine<sup>10,11</sup>, coumarin<sup>12,13</sup>, carbazole<sup>14,15</sup> etc, were widely used as donor moieties in the design of sensitizers, while cyanoacrylic acid was by far the most commonly used anchoring and electron acceptor unit. The structure of  $\pi$ -conjugated bridge can be easily tuned and can comprise a variety of functional units such as phenylenevinylene, benzothiadiazole, thiophene, dithienothiophene, EDOT, selenophene etc<sup>6,16</sup>.

For further development of high performance organic dyes in DSSCs, these have been designed in order to absorb most of the radiation of solar light in visible and near-IR regions and to generate a substantial photocurrent response. In addition, the charge transfer process between the electron donor and acceptor units in the dye must allow the rapid electron injection from the organic dye into the conduction band of the wide band semiconductor, i.e. TiO<sub>2</sub>, which is a very important issue which has to be addressed for obtaining efficient DSSCs. Another distinguishable feature consists in the use of a binary  $\pi$ -conjugated spacer, aside from the blocks of a lipophilic alkoxy-substituted electron-donor (D) and a hydrophilic cyanoacrylic acid electron-acceptor (A).

Triarylamine moiety has been widely used in the design of opto- and electro-active materials due to its good electron donating and transporting ability. Therefore, the functional materials incorporating triarylamine as electron donor unit were intensively explored in the field of solar cells. These

<sup>a</sup> "Petru Poni" Institute of Macromolecular Chemistry, Aleea Gr. Ghica Voda 41A, Iasi-700487, ROMANIA. \*Corresponding author, e-mail: damaceanu@icmpp.ro

<sup>b</sup> Honeywell Romania, Sensors and Wireless Laboratory, 3, George Constantinescu, BOC Tower, 020339 Bucharest, Romania

<sup>c</sup> National Institute for Research and Development in Microtechnologies (IMT), 126A, Erou Iancu Nicolae Street, 077190, Bucharest, Romania

† Electronic Supplementary Information (ESI) available. See DOI: 10.1039/x0xx00000x

materials have significantly enhanced the conversion efficiency of the solar cells, especially of DSSCs<sup>17,18</sup>. Also, the use of thiophene moiety in the conjugated linker was expected to provide a red-shift of the absorption spectra, thus broaden the dye absorption region, which may lead to an appropriate lowest unoccupied molecular orbital (LUMO) energy. On the other hand, it was proved that furan ring can be employed in the dye-sensitized solar cells as a stabilizing unit, enlarging the selection range of building blocks for further dye design. Moreover there is a trade-off between enhanced photocurrent and reduced photovoltage along with the use of electropositive heteroatoms as well as more conjugated units<sup>19</sup>.

To get a better insight into the relationship between dye structure, photo-physical behaviour, electrochemical properties, and the performance of DSSCs based on metal-free sensitizers, a new D- $\pi$ -A organic dye based on dihexyloxy-substituted triphenylamine moiety (**BCS-1**)<sup>20</sup> has been designed, synthesized, and fully characterized for the use in DSSCs. The acronym was chosen as to concord the ones given in the patent. The hexyloxy groups were attached to the triphenylamine to enhance the extent of electron delocalization, thus the ability of electron donating of the sensitizer. An electron spacer containing furan and thiophene moieties were employed in the dye sensitizer for the expansion of the  $\pi$ -conjugated fragment as to adjust the UV –

Vis absorption spectra, as well as the HOMO/LUMO levels of the dye. One C=C bond was introduced in the spacer between the two heterocycles and another one between the spacer and the acceptor unit in order to maintain the extended conjugation level. The organic dye has a cyanoacrylic acid group as electron-withdrawing part and for anchoring onto the TiO<sub>2</sub> surface. The preliminary performances of the novel dye as photosensitizer in DSSCs are also reported.

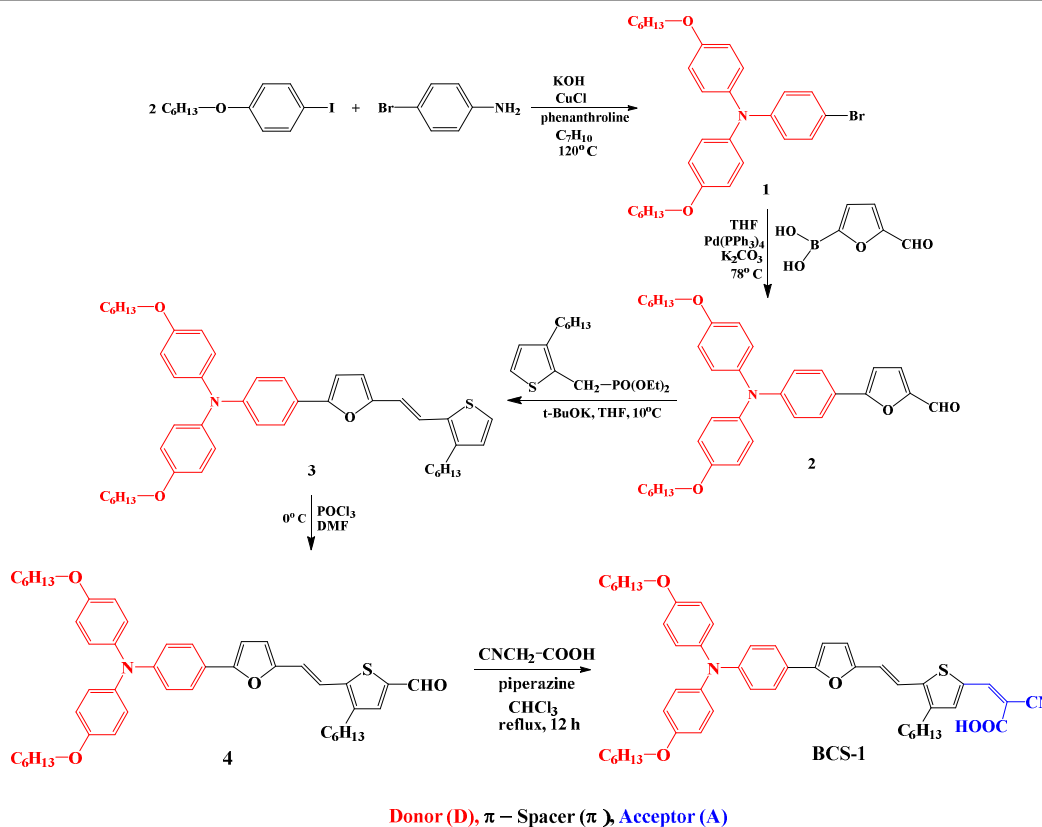
## 2. Experimental Section

### 2.1. Starting materials

Details about starting materials are available in the ESI†. 1-(Hexyloxy)-4-iodobenzene was prepared by the reaction of *p*-iodophenol and 1-bromohexane in DMF, in the presence of K<sub>2</sub>CO<sub>3</sub>, according to literature data<sup>21</sup>. Diethyl-[(3-hexylthiophen-2-yl)methyl]phosphonate was synthesized according to reference<sup>22</sup>, starting from 3-hexylthiophene.

### 2.2. Synthesis

The synthetic pathway to **BCS-1** dye is outlined in scheme 1 and the details are described as follows.



Scheme 1. Synthetic pathway of the **BCS-1** dye (**1**: 4-bromo-N,N-bis(4-(hexyloxy)phenyl)aniline; **2**: 5-(4-(bis(4-(hexyloxy)phenyl)amino)phenyl)furan-2-carbaldehyde; **3**: N,N-bis(4-(hexyloxy-phenyl)-N-(4-(5-(2-(3-hexylthiophen-2-yl)viny)furan-2-yl)phenyl)-aniline; **4**: 3-[5-[2-(5-[4-(bis(4-hexyloxy-phenyl)-amino)-phenyl]-furan-2-yl)-vinyl]-3-hexyl-thiophen-2-yl]-2-carbaldehyde; **BCS-1**: 3-[5-[2-(5-[4-(bis(4-hexyloxy-phenyl)-amino)-phenyl]-furan-2-yl)-vinyl]-3-hexyl-thiophen-2-yl]-2-cyanoacrylic acid)



## Journal Name

## ARTICLE

*4-bromo-N,N-bis(4-(hexyloxy)phenyl)aniline (1)*

In a 100 mL three-necked round-bottomed flask equipped with a magnetic stirring bar and nitrogen inlet and outlet, 1-(hexyloxy)-4-iodobenzene (9.12 g, 30 mmol), 4-bromoaniline (2.064 g, 12 mmol), 1,10-phenanthroline (432 mg, 2.4 mmol) and toluene (50 mL) were placed. The resulting solution was heated at 100°C under vigorous stirring and potassium hydroxide (5.376 g, 96 mmol) and cuprous chloride (237.6 mg, 2.4 mmol) were added under nitrogen. The reaction mixture was refluxed at 120°C overnight (21 h) when the solution became darker (violet), followed by cooling to room temperature. The reaction was quenched with 200 mL water. The crude product was extracted three times with dichloromethane (DCM), and the combined organic layer was washed with water and dried over anhydrous sodium sulphate. After removing the solvent under reduced pressure, the oil residue was purified by column chromatography using hexane successively hexane and hexane: ethyl acetate 30/1, v/v to obtain a brown oil (3.1g, 51% yield). <sup>1</sup>H-NMR (DMSO, 400 MHz), δ (ppm): 7.31-7.28 (d, 2H), 7.01-6.99 (d, 4H), 6.90-6.88 (d, 4H), 6.67-6.65 (d, 2H), 3.92 (t, 4H), 1.69 (m, 4H), 1.39 (m, 4H), 1.31 (m, 8H), 0.889 (t, 6H).

*5-(4-(bis(4-(hexyloxy)phenyl)amino)phenyl)furan-2-carbaldehyde (2)*

3.05 g (5.997 mmol) of 1 dissolved in 10 mL anhydrous THF, 1.148 mg (8.208 mmol) 5-formyl-2-furanboronic acid and 85 mL anhydrous THF were placed in a Schlenk tube under strong nitrogen stream. The resulting solution was stirred at room temperature under nitrogen for several minutes, after that 35 mL aqueous K<sub>2</sub>CO<sub>3</sub> solution (2M) and 250 mg (0.216 mmol) Pd(PPh<sub>3</sub>)<sub>4</sub> were added when the colour changed to green-black. The reaction mixture was stirred at 78°C overnight, cooled down to room temperature, and quenched with 20 mL water. The crude product was extracted three times with DCM, and the combined organic layer was washed with water and dried over anhydrous sodium sulphate. After removing the solvent under reduced pressure, the residue was purified by column chromatography (hexane: ethyl acetate 30/1, v/v and hexane: ethyl acetate 7/3, v/v) to afford a viscous yellow-green oil (1.114 g, 35.6 % yield). <sup>1</sup>H-NMR (DMSO, 400 MHz), δ (ppm): 9.51 (s, 1H), 7.66-7.64 (d, 2H), 7.61-7.60 (d, 1H), 7.11-7.09 (d, 4H), 7.04-7.03 (d, 1H), 6.96-6.93 (d, 4H), 6.78-6.76 (d, 2H), 3.95 (t, 4H), 1.71 (m, 4H), 1.40 (m, 4H), 1.32 (m, 8H), 0.90 (t, 6H).

*N,N-bis(4-(hexyloxy-phenyl)-N-(4-(5-(2-(3-hexylthiophen-2-yl)vinyl)furan-2-yl)phenyl)-aniline (3)*

326 mg (2.903 mmol) t-BuOK were placed in a Schlenk tube, dried under vacuum and purged with nitrogen, after that 17 mL dry THF were added and cooled in an ice bath. 851.6 mg (2.68 mmol) of diethyl [(3-hexylthiophen-2-yl)methyl]-

phosphonate dissolved in 17 mL anhydrous THF were introduced dropwise in the flask under strong stirring, being accomplished by colour change to dark-red. Then, 1.168 g (2.233 mmol) of 2 dissolved in 20 mL anhydrous THF was added dropwise for 30 minutes under nitrogen stream while maintaining the flask in the ice bath. The temperature was allowed to reach 25°C and stirring was continued for another 3 hours. The reaction was not quenched with water nor processed by extraction. The resulting mixture was brought to dryness and further purified by column chromatography using successively hexane: ethyl acetate 9/1, v/v and hexane: ethyl acetate 7/3, v/v, to yield a viscous red-brown oil (1.037 g, 67% yield). <sup>1</sup>H-NMR (CDCl<sub>3</sub>, 400 MHz), δ (ppm): 7.50-7.48 (d, 2H), 7.13-7.09 (d, 1H), 7.06-7.04 (d, 4H), 6.94 - 6.92 (d, 2H), 6.88 (s, 1H), 6.83-6.81 (d, 4H), 6.75 (s, 1H), 6.70-6.64 (d, 1H), 6.50-6.49 (d, 1H), 6.35-6.34 (d, 1H), 3.94 (t, 4H), 2.55 (t, 2H), 1.77 (m, 4H), 1.60 (m, 2H), 1.46 (m, 4H), 1.36-1.24 (m, 14H), 0.90 (m, 9H).

*3-[5-[2-(5-[4-(bis(4-(hexyloxy-phenyl)-amino)-phenyl]-furan-2-yl)-vinyl]-3-hexyl-thiophen-2-yl]-2-carbaldehyde (4)*

In a Schlenk tube, Vilsmeier reactive was prepared under nitrogen stream and stirring by dropping 925.35 mg (6.04 mmol, 0.56 mL) POCl<sub>3</sub> over 441.5 mg (6.04 mmol) anhydrous DMF maintained in an ice bath for 5-10 minutes. After occurrence of a slightly opaque ice, 35 mL dichloroethane was added to the Vilsmeier reactive and the stirring continued for 1 hour at 0°C, when a white opalescent solution was obtained. To this solution, 842 mg (1.225 mmol) of 3 dissolved in 35 mL dichloroethane was added dropwise under nitrogen stream for 30 minutes. Then, the reaction was run 4 hours at 0°C and quenched with cold water. Neutralization was done by extracting the reaction mixture with saturated sodium bicarbonate solution to turn the colour from purple to orange-red, when the organic phase was extracted with DCM and wash with water. After drying over anhydrous sodium sulphate and the solvent evaporation under reduced pressure the residue was purified by column chromatography using hexane: ethyl acetate 9/1, v/v, affording a reddish-brown clay (750 mg, 86% yield). <sup>1</sup>H-NMR (DMSO, 400 MHz), δ (ppm): 9.98 (s, 1H), 7.62-7.59 (d, 2H), 7.29 (s, 1H), 7.18 (s, 1H), 7.12 (s, 1H), 7.06-7.04 (d, 4H), 6.94 - 6.92 (d, 4H), 6.85-6.84 (d, 1H), 6.80-6.78 (d, 2H), 6.77-6.76 (d, 1H), 3.95 (t, 4H), 2.93 (t, 2H), 1.71 (m, 4H), 1.63 (m, 2H), 1.42 (m, 4H), 1.36-1.24 (m, 14H), 0.89 (m, 9H).

*3-[5-[2-(5-[4-(bis(4-(hexyloxy-phenyl)-amino)-phenyl]-furan-2-yl)-vinyl]-3-hexyl-thiophen-2-yl]-2-cyanoacrylic acid (BCS-1)*

In a Schlenk tube, 633 mg (0.885 mmol) of 4 dissolved in 10 mL chloroform and 225.9 mg (2.656 mmol) of cyanoacetic acid were placed. This mixture was stirred for 10 minutes under nitrogen stream, and then 527.6 mg (6.196 mmol, 0.61 mL)

piperidine was added dropwise to the mixture and other 23 mL of chloroform. The reaction mixture was kept under stirring and gentle reflux (65 °C) for 12 h. The reaction was quenched with 75 mL HCl 2M, when the colour turned from cherry-red to purple. The organic phase was extracted 3 times with DCM and washed three times with water as the last washing water to have pH = 5.5. After drying over Na<sub>2</sub>SO<sub>4</sub> and solvent evaporation, the residue was purified by column chromatography using successively DCM and DCM: methanol 10/1, v/v, to afford a purple powder (470 mg, 61.8% yield). <sup>1</sup>H-NMR (DMSO, 400 MHz), δ (ppm): 8.17 (s, 1H), 7.62-7.60 (d, 2H), 7.28 (s, 1H), 7.24-7.00 (d, 1H), 7.20 (s, 1H), 7.05-7.03 (d, 4H), 6.93 - 6.91 (d, 4H), 6.85-6.84 (d, 1H), 6.80 (s, 1H), 6.79-6.78 (d, 2H), 3.95 (t, 4H), 2.71 (t, 2H), 1.71 (m, 4H), 1.58 (m, 2H), 1.42 (m, 4H), 1.33-1.24 (m, 14H), 0.90 (m, 9H). <sup>13</sup>C-NMR (CDCl<sub>3</sub>, 100 MHz), δ (ppm): 168.66, 155.79, 155.50, 150.98, 148.69, 143.66, 140.33, 129.34, 128.06, 126.80, 124.99, 122.20, 120.02, 117.59, 115.42, 114.67, 106.21, 68.36, 67.95, 43.42, 31.93, 31.62, 30.90, 29.69, 29.35, 28.98, 25.77, 25.61, 22.67, 22.60, 22.53, 14.05, 13.99. MS (ESI, m/z): calc for C<sub>34</sub>H<sub>24</sub>N<sub>4</sub>O<sub>3</sub>, 798.4066; found, 797.3412 [M - H]<sup>-</sup>.

### 2.3. Preparation of dye coatings

Very diluted dye solutions in DCM with concentration of 0.5-1 % weight were used to obtain thin coatings having the thickness in the range of nanometers onto glass and ITO-coated glass substrates by drop-casting technique. The as-prepared dye solutions were filtered through a 0.45 μm filter before drop-casting. In order to remove the residual solvent, these coatings were gradually heated from room temperature up to 50 °C, and kept at 50 °C for 3 h and were used afterwards for UV-Vis, fluorescence and electrochemical properties investigations.

### 2.4. Measurements

The <sup>1</sup>H- and <sup>13</sup>C-NMR spectra were recorded on a BrukerAvance III 400 spectrometer, equipped with a 5 mm multinuclear inverse detection probe, operating at 400.1 and 100.6 MHz for <sup>1</sup>H and <sup>13</sup>C nuclei, respectively. <sup>1</sup>H and <sup>13</sup>C chemical shifts are reported in δ units (ppm) relative to the residual peak of the solvent.

Mass spectral (MS) data were collected on an Agilent 6520 Accurate Mass ESI Q-ToF Liquid Chromatography/Mass Spectrometer.

The infrared (FTIR) spectra were registered with a FTIR Bruker Vertex 70 Spectrophotometer in transmission mode by using KBr pellets.

The UV-Vis absorption and photoluminescence spectra were recorded at room temperature on Specord M42 and Perkin Elmer LS 55 instruments, respectively, by using very diluted dye solutions (≈ 10<sup>-5</sup> M) in DCM or DMF and very thin coatings on glass plates.

Electrochemical properties of the dye were investigated by cyclic voltammetry (CV) which was performed on a Bioanalytical System, Potentiostat-Galvanostat (BAS 100B/W).

The electrochemical cell was equipped with three-electrodes: a working electrode (ITO-coated glass covered with the dye or platinum), an auxiliary electrode (platinum wire) and a reference electrode (silver wire coated with AgCl). Tetrabutylammonium perchlorate (TBAP)/acetonitrile was used as supporting electrolyte for the dye coating samples and TBAP/DCM or TBAP/DMF for solution samples having the concentration of 1×10<sup>-3</sup> M. All potentials were reported with respect to Ag/AgCl electrode under ambient conditions, at the scan rate of 50 mV/s. Ferrocene was used as an external reference for calibration (+0.425 vs Ag/AgCl).

### 2.5. Solar cell fabrication and characterization

A 10 μm TiO<sub>2</sub> mesoporous layer was screen printed on a dense TiO<sub>2</sub> barrier layer, grown on the FTO conducting glass (Solaronix, Aubonne, Switzerland). Then, a 4 μm scattering layer was grown on the mesoporous layer. Both layers were treated in a TiCl<sub>4</sub> atmosphere. The TiO<sub>2</sub> film was functionalized using a 0.3 mM solution of the dye. Different solvents or solvent combinations have been used to prepare the functionalization solutions; the immersion time has been varied between 2.5 and 16 h. Samples with and without additive (chenodeoxycholic acid, CDCA) were prepared. In some experiments, the TiO<sub>2</sub> film was re-fired at 450 °C, for 30 minutes, slowly cooled and immersed into the functionalization solution at 80 °C. After functionalization, the film was fully rinsed with ethanol and soaked in nitrogen flux. A platinized FTO was used as counter electrode (Solaronix). The functionalized TiO<sub>2</sub> film was encapsulated using a platinum counter electrode with a Surlyn sealant (Solaronix). A hole practiced into the counter electrode was used to introduce the electrolyte. The hole was sealed by heating using a Surlyn sheet and a small glass cover. Two different commercial electrolytes (HI-30 and AN-50, Solaronix) were used, both based on I<sup>-</sup>/I<sub>3</sub><sup>-</sup> redox couple, with two different I<sub>3</sub><sup>-</sup> concentrations, 30 mM (HI-30) and 50 mM (AN-50), with ionic liquid, lithium salt and pyridine derivative used as additives and acetonitrile as solvent. The device area was 0.36 cm<sup>2</sup>. The current-voltage (I-V) characteristics of the cells were recorded using a Keithley I-V tracer, while samples were illuminated with broad band ozone-free Xe source through a standard AM1.5G filter, at a power density of 1 Sun (100 mW/cm<sup>2</sup>) measured by a National Institute of Standards and Technology traceable thermopile detector. The interfacial transfer processes have been analyzed using the electrochemical impedance spectroscopy (EIS) technique, under dark and illumination conditions. The EIS measurements were performed on a PARSTAT 2273 (Princeton Applied Research), under constant light illumination of 0.14 Sun. The spectra were recorded over a frequency range from 10 mHz to 500 kHz with logarithmic point spacing, at a low AC amplitude of 10 mV (RMS) to maintain the response linearity in open circuit conditions.

### 2.6. Computational calculations

A slightly modified molecular structure of **BCS-1** was used for simulations - **BCS-1m** (whose structure is shown in ESI†, figure S6), in which the hexyl groups were replaced by methyl units to avoid geometry optimization difficulties due to the floppiness of the long alkyl chains. The geometry of **BCS-1m** was optimized using the density functional theory (DFT) with the B3LYP exchange-correlation functional<sup>23,24</sup> and 6-311++G\*\* basis set<sup>25-27</sup>. This approach for geometry optimization has been noted to be robust<sup>28</sup>.

The UV-Vis spectrum of the dye was simulated by computing the excited states using the time-dependent (TD) DFT with the CAM-B3LYP functional and the 6-311++G\*\* basis set using the B3LYP/6-311++G\*\* optimized geometry. CAM-B3LYP<sup>29</sup> is a range-separated hybrid functional and it has been found to successfully describe charge-transfer excited states<sup>30,31</sup>.

All DFT and TD-DFT calculations were performed using Gaussian09<sup>32</sup>; molecular and orbitals figures, along with UV-Vis spectra were produced using GaussView Version 5<sup>33</sup>.

### 3. Results and discussion

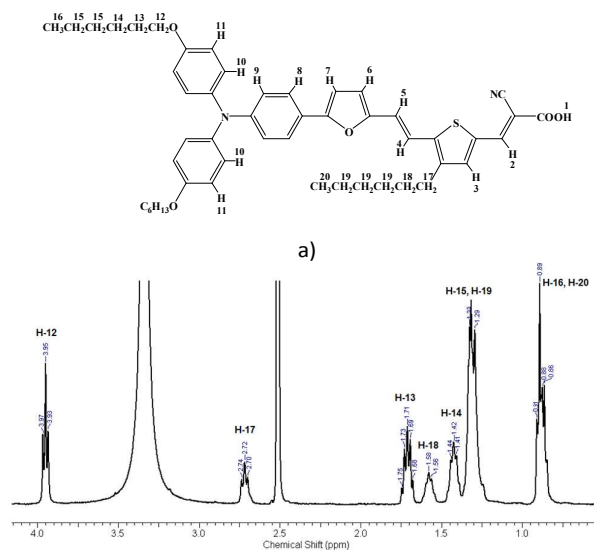
#### 3.1. Synthesis and structural characterization of BCS-1 dye

The new sensitizer combines some structural features which are usually encountered in the design of other dyes: the triphenylamine containing two hexyloxy substituents as donor moiety, the linker containing both thiophene and furan rings connected through a vinylene bridge, and the cyanoacrylic acid used both as anchoring group and electron acceptor. A long alkyl chain on the thiophene ring was attached in order to suppress the aggregation and minimize the recombination<sup>34</sup>. The cyanoacrylic acid group is essentially coplanar with respect to the thiophene unit, reflecting the strong conjugation across the linker and the anchoring group. Thus, the electrons distribution is accomplished: they move from the triphenylamine moiety through the  $\pi$ -conjugated furan-vinylthiophene bridge to the cyanoacrylic acid acceptor by means of photoexcitation of the dye (a  $\pi$ - $\pi^*$  transition), and then are injected to the conduction band of TiO<sub>2</sub> via the anchoring carboxyl group. This photoexcitation-induced intramolecular charge transfer occurring in the **BCS-1** dye is analogous to that taking place in a Ru-complex photosensitizer and leads to a high electron-injection yield into the conduction band of TiO<sub>2</sub> and, consequently, to an efficient charge separation in the system. Therefore, the molecular structure of our organic-dye photosensitizer suggests that it is promising for use in DSSCs; thus the preliminary results of its performance are reported.

The **BCS-1** dye was characterized by FTIR, <sup>1</sup>H- and <sup>13</sup>C-NMR spectroscopy, thereby fully proving its chemical structure. In FTIR spectrum the dye exhibits characteristic absorption bands of the carboxylic functional group at 3443 cm<sup>-1</sup> (OH stretching, wide band) and 1712 cm<sup>-1</sup> (C=O stretching), as well as of the CN group at 2211 cm<sup>-1</sup>. The incorporation of furan ring into the dye was evidenced by the medium-strong bands at 1021

cm<sup>-1</sup> and 967 cm<sup>-1</sup> attributed to the =C-O-C= vibration or heteroatom ring deformation of the furan ring. The band from 3039 cm<sup>-1</sup> is assigned to the C-H stretching on phenylene units, while the system band from 2954-2853 cm<sup>-1</sup> corresponds to aliphatic C-H stretching of the alkyloxy and alkyl lateral groups of the dye. The bands at 1601 and 1505 cm<sup>-1</sup> were assigned to aromatic C=C stretching in thiophene, furan and phenylene rings, while the band at 1239 cm<sup>-1</sup> were associated with the C-O-C stretching in hexyloxy units. Vibrations at 1480, 1414, 1261 and 1164 cm<sup>-1</sup> originate from the stretching of C-C and C=C bonds in the thiophene ring. Further IR bands corresponding to the C-S bond in the thiophene ring can be found at 825 cm<sup>-1</sup>. The FTIR spectrum of **BCS-1** dye is available in ESI† (figure S1).

In the <sup>1</sup>H-NMR spectrum (figure 1) the proton belonging to the thiophene ring was evidenced by the singlet at 7.29 ppm (H-3), whereas the protons of the furan unit (H-6,H-7) gave splitted patterns that are partially overlapped with the signals corresponding to the aromatic protons of the triphenylamine (H-11). The protons belonging to the phenylene units fall at 7.62-7.60 ppm (d, H8), 7.06-7.03 (d, H-11), 6.94-6.91 (d, H-10) and 6.78 ppm (H-9, overlapped signals). The most shielded signal at 8.17 ppm was attributed to the proton H-2 of cyanoacrylic acid. The two doublets from 6.85-6.84 and 6.80-6.79 ppm were assigned to the protons H-4 and H-5, respectively, of the vinylene bridge between thiophene and furan rings. The protons belonging to the hexyloxy groups were evidenced by the triplet at 3.96-3.93 ppm (H-12) and the multiplets at 1.75-1.68 ppm (H-13) and at 1.44-1.41 ppm (H-14), while the methylene protons H-17 and H18 of the hexyl group appeared at 2.74-2.70 ppm (triplet) and 1.58-1.56 ppm (multiplet), respectively. All the other aliphatic protons (H-15, H-16, H-19, H-20) of these groups gave overlapped signals at 1.33-1.24 ppm and 0.91-0.86 ppm. In the <sup>13</sup>C-NMR spectrum the presence of carboxylic group in the **BCS-1** dye was evidenced by the most shielded signal at 168.66 ppm, while the nitrile group appeared at 117.59 ppm (figure S2, ESI†).



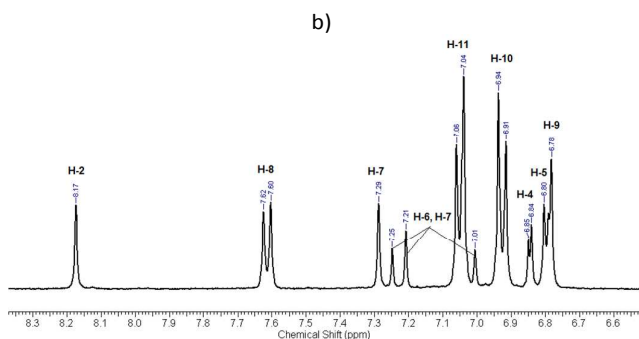


Figure 1.  $^1\text{H-NMR}$  spectrum of **BCS-1** dye (a: aliphatic region, b: aromatic region)

### 3.2. Photo-physical properties

The optical properties of the **BCS-1** dye were assessed on the basis of UV-Vis absorption and photoluminescence spectra recorded for both solutions and coatings, after irradiation with UV light of various lengths corresponding to each absorption maxima, with a special concern on the solvent effect.

The prominent feature of this oligomer material is its extended conjugated  $\pi$  system; such extension of conjugation is reflected in the electronic absorption spectrum. Figure 2 displays the absorption spectra of **BCS-1** dye in DCM solution and solid state in comparison with the simulated one (TD CAM-B3LYP/6-311++G\*\*).

It was found that both in solution and in solid state, **BCS-1** exhibited a structured band in the lower energy region, centred at 507 and 516 nm, respectively, and a less intense peak in the UV domain, at 366 nm (DCM solution) and 368 nm (film). An additional absorption peak in solution was also detected at 303 nm. The absorption bands in the lower energy region are assignable to the  $\pi$ - $\pi^*$  transition resulting from the conjugation between the triphenylamine moiety and cyanoacrylic unit through the  $\pi$ -conjugated furan-vinylthiophene bridge.

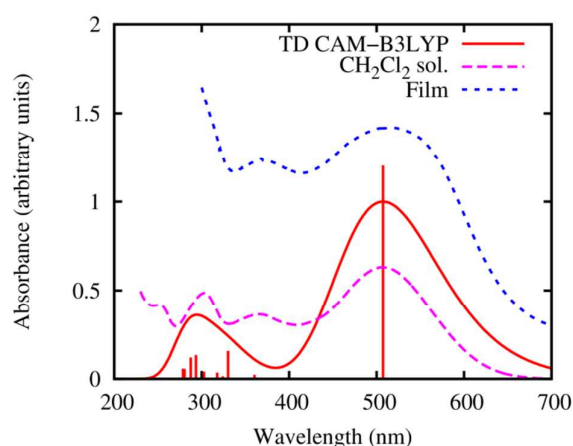


Figure 2. Recorded UV-Vis spectra of **BCS-1** in  $\text{CH}_2\text{Cl}_2$  solution and solid state compared with simulated UV-Vis spectrum of **BCS-1m**

The origin of this electronic absorption was confirmed by calculating the singlet electronic transitions using TD-DFT. TD

CAM-B3LYP/6-311++G\*\* calculations proved that this visible band originates intrinsically from the intramolecular charge-transfer transition from the highest occupied molecular orbital (HOMO) to the lowest unoccupied molecular orbital (LUMO). There is no important change observed between the DCM solution and solid state absorption. In solid state, the UV-Vis absorption spectrum of **BCS-1** dye showed a broadening compared with its solution, the maximum from the lower energy region being red-shifted with 9 nm compared with the absorption of isolated molecules (figure 2). The dye is likely in an aggregated state in DCM solution, and therefore the absorption does not shift an appreciable amount upon evaporation of the solvent into a thin film. It seems that this solvent favours strong  $\pi$ - $\pi$  interactions between dye molecules, the molecules being predominantly in planar conformations. This statement is sustained by a strong blue shift (45 nm) of the main absorption maximum of **BCS-1** dye in DMF solution, proving that the dye molecules lose conjugation in this solvent (*Supporting Information*, figure S3). The solvated dye molecules are more disordered, showing that solvent-solute interactions are prevalent in DMF solution. In fact, this is easily visible to the naked eye: the DCM solutions are deep purple coloured, while DMF solutions are of orange-red colour. This is a simple example to prove that the absorption spectra of **BCS-1** dye is highly solvent sensitive, demonstrating that the solar cell engineering strategy will be the most important feature in achieving good power conversion efficiency.

The absorption edge ( $\lambda_{\text{edge}}$ ), being a long-wavelength wing of the longest-wavelength band of the spectrum, moves to longer wavelength (smaller energy) for the dye coatings when compared with the absorption edge of solutions, as a consequence of different molecule conformation in dependence on the surroundings. The optical energy band gap ( $E_{\text{g}}^{\text{opt}}$ ) could be estimated from the following equation:

$$E_{\text{g}}^{\text{opt}} = \frac{hc}{\lambda_{\text{edge}}}$$

where  $h$  is the Planck constant,  $c$  is the light velocity, and  $\lambda_{\text{edge}}$  is the wavelength of the absorption edges of the optical absorption spectra. Thus, the optical energy band gap values corresponding to this compound are of 1.81 eV for the coating, and 1.95 eV and 2.24 eV, for DCM and DMF solutions, respectively. The  $E_{\text{g}}^{\text{opt}}$  values of **BCS-1** dye decrease with the increasing of the conjugation level that is mirrored by the nature and degree of aggregation.

The photoluminescence (PL) spectra were recorded for both solutions and coatings, at the excitation wavelength corresponding to each peak from UV-Vis spectra. Figure 3 displays the PL spectra recorded by excitation with the wavelength corresponding to the absorption maximum from the lower energy region (507 and 463 nm for the DCM and DMF solution, respectively, and 516 nm for the coating).

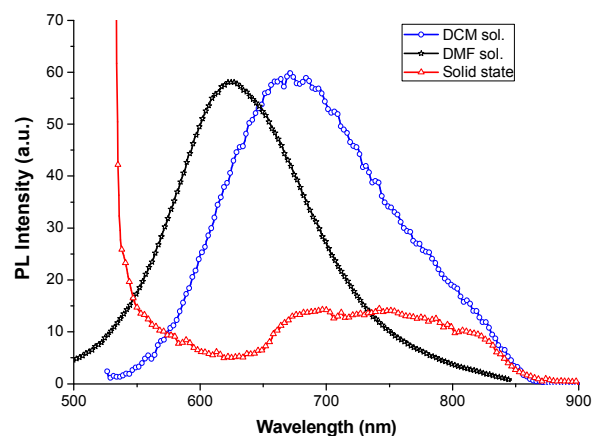


Figure 3. PL spectra of **BCS-1** obtained by excitation with the wavelength corresponding to the main UV-Vis maximum

A PL band in the red region, centred at 675 nm for the DCM solution and 625 nm for the DMF solution was registered, while a broad and weak emission without a clear maximum, centred at  $\approx$  730 nm was obtained for the dye coating. Irradiation with the wavelength corresponding to the middle absorption peak (approx. 360 nm) resulted in PL spectra with a maximum at 664 nm for DCM solution, and no peak for the solid state. In DCM solution, a red shift of the emission maximum was registered as compared to the same dye in DMF solution due to the better  $\pi$ -electrons delocalization between the triphenylamine moiety and cyanoacrylic unit through the  $\pi$ -conjugated furan-vinyl-thiophene bridge. Since the dye bears electron donor and acceptor groups, a charge transfer probably occurs in the excited state from the electron-donor to the electron-acceptor group through the conjugation core. The shape of the emission spectra undergoes a slight change by excitation at 360 nm, suggesting that the change of solvent polarity exerts an impact on the emissive center. It is noteworthy to mention the splitting of the emission band in DMF solution in two peaks, at 547 and 606 nm, due to the coiled conformations gained by the dye in this solvent that impart the conjugated core in two individual fluorophores. A new emission peak appears, indicating that the charge transfer process is suppressed in this solvent. Excitation with the wavelength corresponding to the highest energy absorption peak (approx. 300 nm for both solutions and film) produced no fluorescence in DCM solution and film, and a weak emission peak at 540 nm in DMF solution. Figure S4 (ESI<sup>†</sup>) provides the PL spectra of the **BCS-1** dye registered by excitation at 360 nm in DCM and DMF solution.

### 3.3. Theoretical calculations

The effect of molecular structure and electron distribution of **BCS-1** on the performances of dye-sensitized solar cells were surveyed by optimization of its geometry and HOMO – LUMO energies by using density functional theory (DFT) calculation at the B3LYP/6-311++G\*\* level with Gaussian09 (details in ESI<sup>†</sup>).

According to the optimized geometry of the **BCS-1** dye (figure 4), the benzene rings in the triphenylamine core are non-planar and could reduce the contact between molecules. Triphenylamine has a propeller shape, with the dihedral angles highlighted in figures 4b and 4c of  $\approx$ 50°. The two hexyloxy substituents of the head of the molecule act just like two umbrellas, to maintain a certain distance between the dye molecules when absorbed on TiO<sub>2</sub>. Moreover, the long alkyl chain attached on the thiophene ring is expected to disturb the tight packing of the dye molecules in  $\pi$ -stacks, thus suppressing the aggregation.

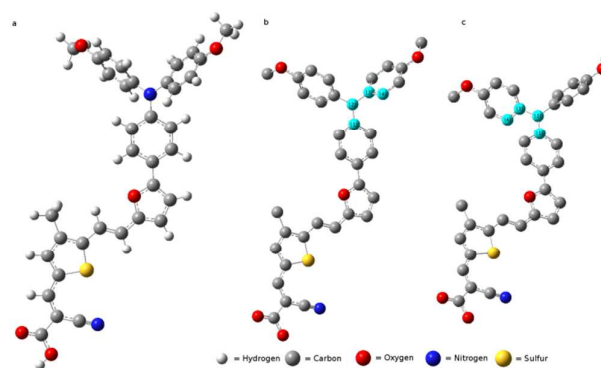
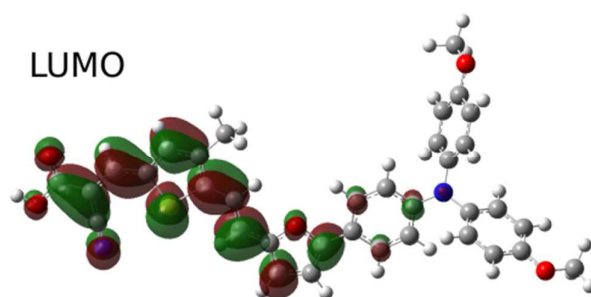
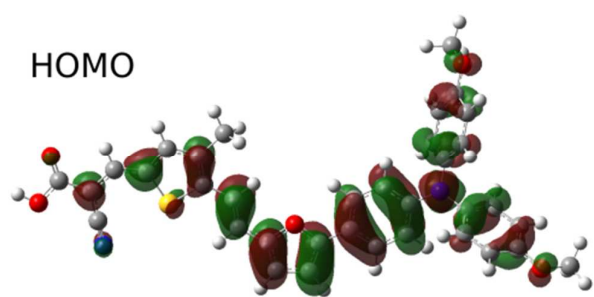


Figure 4. (a) Optimized geometry of **BCS-1m**; (b) and (c) two dihedral angles between the benzene rings in the triphenylamine group showing the propeller shape (hydrogen atoms hidden for clarity in b and c).

Figure 5 shows the frontier orbital plots of the HOMOs and LUMOs of **BCS-1** dye. The HOMO orbital is delocalized in large extent over the donor part - dihexyloxy-substituted triphenylamine moiety and the conjugated bridge (furan-vinyl-thiophene core), while LUMO is mainly located in the electron withdrawing group - cyanoacrylate moiety through the  $\pi$ -spacer, giving the strongest D-A strength. Thus, the HOMO to LUMO excitation induced by light irradiation could move the electron distribution from the whole molecule to the anchoring moiety. As depicted above, it also revealed that the heteroaromatic  $\pi$ -spacer is essentially coplanar with the cyanoacetic acid group, demonstrating an increased delocalization of the electrons between donor and acceptor units. Furthermore, the location of the LUMO next to the TiO<sub>2</sub> surface and the HOMO at the opposite side of the molecule dye causes an easier electron injection into the semiconductor and prevents back regeneration of the dye with injected electrons.

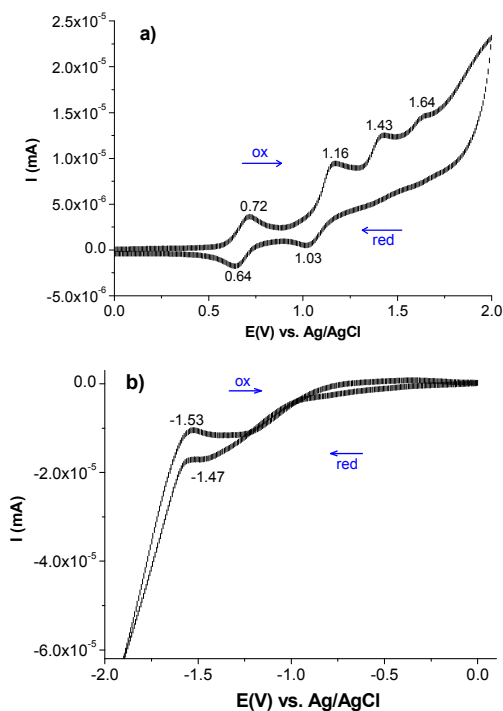


Figure 5. Frontier orbitals of **BCS-1** dye computed with CAM-B3LYP/6-311++G\*\*

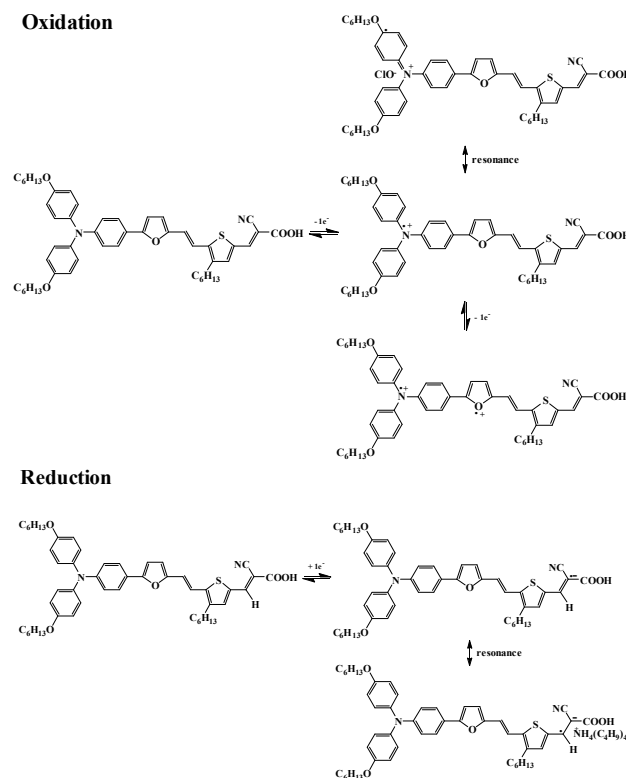
### 3.4. Electrochemical properties

To judge the possibilities of electron transfer from the excited **BCS-1** dye molecule to the conductive band of TiO<sub>2</sub> and the dye regeneration, its redox behaviour in solution and solid state was investigated by cyclic voltammetry (CV): (1) in DCM or DMF solution using Pt as working electrode and (2) as coatings deposited on glass substrates coated with ITO as working electrode.

The cyclic voltammogram of **BCS-1** dye in the first CV cycle recorded in DCM solution containing TBAP as electrolyte, in ambient conditions, is shown in figure 6. By scanning the potential in the anodic direction, four oxidation and two reduction peaks were registered. The **BCS-1** dye undergoes in the first scan a reversible redox process arising from triphenylamine unit followed by a series of quasireversible or irreversible oxidations originating from  $\pi$ -bridged aromatic moieties.

Figure 6. Cyclic voltammogram of **BCS-1** in solution (a: anodic scan, b: cathodic scan)

The first oxidation peak, occurring at  $E_{ox1} = 0.72$  V, is caused by the formation of the triphenylamine cation radicals. Due to the strong electron releasing properties of hexyloxy groups toward the tri-arylamine moiety, the **BCS-1** dye exhibits the oxidation process at a much lower potential value than the corresponding tri-arylamines without alkyl groups that usually give one oxidation peak at 1–1.2 V<sup>35</sup>. The redox process and the resonance forms of **BCS-1** are displayed in scheme 2.

Scheme 2. The simplified redox mechanism of **BCS-1** from neutral to dication state

When **BCS-1** molecules were oxidized to their cationic state, the molecules would possess positive charge and the corresponding anions from the electrolyte solution (ClO<sub>4</sub><sup>-</sup>) would insert into the molecules and neutralize the charge. After first step of oxidation, resonant reactions may occur and the radical state of N<sup>•+</sup> would resonate to the phenyl group.

The further oxidation process revealed three anodic peaks at  $E_{ox2} = 1.16$  V,  $E_{ox3} = 1.43$  V, and  $E_{ox4} = 1.64$  V. The second peak can be ascribed to the formation of dication resulted upon subsequent oxidation, most probably of the furan unit, being followed by the oxidation of the  $\pi$ -conjugated system (scheme 2). The oxidation of thiophene ring cannot be taken into consideration since it is substituted with the strong electron-withdrawing cyanoacrylic group and is more susceptible for the reduction process<sup>36</sup>. Generally, by increasing the conjugation and the number of electroactive sites, a higher electronic delocalization is attained which may cause differences in redox behavior of the derivatives due to the generation of specific electrochemical species<sup>37</sup>. Such feature is sustained by the absence of the 3<sup>rd</sup> and 4<sup>th</sup> oxidation peaks

when the CV was performed in DMF solution, in perfect agreement with the UV-Vis data. In DMF, the conjugation of **BCS-1** dye decreased and a lower electronic delocalization occurred, leading to less redox sites. Moreover, the oxidation peaks registered in DMF solution due to the formation of radical cations and dications are positively shifted compared to DCM solution, at  $E_{ox1} = 0.77\text{V}$  and  $E_{ox2} = 1.19\text{V}$ , respectively. The positive shift of the anodic peak is associated with a distortion of the  $\pi$ -conjugated system, and is usually accompanied by a blue shift of the UV-Vis absorption maximum<sup>38</sup>.

On the reverse scanning, two reduction processes occurred in DCM solution, at  $E_{red1} = 1.03\text{V}$  and  $E_{red2} = 0.64\text{V}$ , whereas one clear reduction peak at  $E_{red} = 0.29\text{V}$  was registered in DMF solution. The intensity of the redox peaks decreased with increasing the number of scans in DCM solution, indicating that the oxidation process is stable only at the triphenylamine moiety, while the other electrochemical species deactivated upon multiple scanning the potential in the anodic direction (figure 7). Instead, a very good stability of redox processes was observed in DMF solution (ESI†, figure S5). In the cathodic region, one reduction peak at  $-1.47\text{V}$  and  $-1.15\text{V}$  in DCM and DMF solutions, respectively, was registered, being attributed to the formation of radical anions of the electron-withdrawing cyanoacrylic unit that undergoes subsequent oxidation at  $-1.53\text{V}$  only in DCM solution (scheme 2). During the repetitive potential swept the reduction step remained very stable in DCM solution since no change in the position of the cathodic peak was observed.

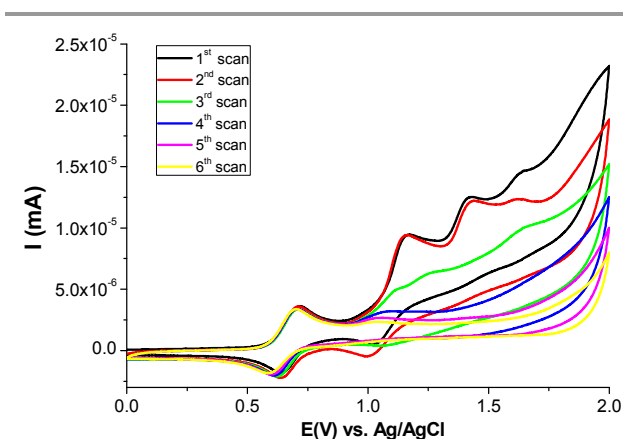


Figure 7. Electrochemical stability of **BCS-1** in solution over six subsequent scans

Evaporation of a drop of diluted dye solutions in DCM with concentration of 0.5 % onto an ITO electrode should result in the formation of strong bonds between the carboxylate groups of the dye and ITO<sup>39</sup>. Characteristic surface waves are recorded near the potentials of the solution waves after the evaporation step (ESI†, figure S5). Only two large oxidation waves were registered in the anodic region, being centred at 0.94 and 1.44 V. The first step was associated with the formation of radical cations of triphenylamine unit, while the second one may be assigned to the oxidation of furan moiety. Two reduction steps at 1.38 and 0.63 V, assigned to the reduction of the formed

radical cations during the oxidation process, were observed as well. In the cathodic region, an inflection at  $-1.59\text{V}$  appeared being associated with the reduction of cyanoacrylic moiety, without a peak corresponding to its oxidation. The electrochemical stability of **BCS-1** dye in solid state was not possible to be evaluated since the films stripped off from the electrode after the first CV wave, most probably due to the dissolution of non-covalently attached **BCS-1** dye molecules from the electrode surface after the current flow.

Knowing the HOMO and LUMO energy levels is crucial for the choice of materials that can form an appropriate interface for configuration of the photovoltaic cells from the energetic point of view. The energy levels of the highest occupied molecular orbital (HOMO) and lowest unoccupied molecular orbital (LUMO) of the investigated **BCS-1** dye can be more precisely evaluated from the oxidation onset potentials ( $E_{onset}^{ox}$ ) and reduction onset potentials ( $E_{onset}^{red}$ ) versus Ag/AgCl. The onset potentials were determined from the intersection of the two tangents drawn at the rising current and baseline charging current of the CV curves. The external ferrocene/ferrocenium ( $F_c/F_c^+$ ) redox standard  $E_{onset}$  is  $0.425\text{V}$  versus Ag/AgCl. Assuming that the HOMO energy for the  $F_c/F_c^+$  standard was  $4.80\text{eV}$  with respect to the zero vacuum level, we can estimate the HOMO and LUMO energy levels, and the energy bandgap ( $E_g$ ) (in electron volts, eV) according to the following equations:

$$E_{LUMO} = E_{onset}^{red} + 4.37, \quad E_{HOMO} = E_{onset}^{ox} + 4.37$$

$$E_g = E_{HOMO} - E_{LUMO}$$

The HOMO energy level was calculated to be  $4.96\text{eV}$  for **BCS-1** dye in solution and  $4.92\text{eV}$  in solid state, while the LUMO energy value reaches  $3.34\text{eV}$  for solution and  $3.41\text{eV}$  for coating. Thus, the resulted values for the energy bandgap of **BCS-1** dye are  $1.62\text{eV}$  and  $1.51\text{eV}$ , for DCM solution and coating, respectively. A small disparity was observed between the band gap energy values measured by spectroscopic and electrochemical methods. There is no conflict between these values, since they describe distinct processes. The spectroscopic measurements provide an estimation of the energy difference of the frontier orbitals and the obtained optical band gap corresponds to the energy required to form a tightly-bound exciton, whereas the redox potentials give the absolute energetic positions of the HOMO and LUMO levels and the electrochemical or transport band gap corresponds to the energy required to form free charge carriers<sup>40</sup>.

The energy barriers between the **BCS-1** dye and electrodes can be estimated by comparing the edge of the conduction band of  $\text{TiO}_2$  and the potential of the redox couple ( $I/I_3^-$ ) with its HOMO and LUMO energy levels. Thus, the hole injection barrier is  $\Delta E_h = E_{HOMO} - 4.8\text{eV}$  ( $4.8\text{eV}$  is the redox couple of  $I/I_3^-$  vs. vacuum), whereas the electron injection barrier is  $\Delta E_e = 4.0 - E_{LUMO}$  (eV), ( $4.0\text{eV}$  is the edge of the conduction band of  $\text{TiO}_2$  vs. vacuum)<sup>41-43</sup>. The band structure of **BCS-1** dye is depicted in figure 8. It can be observed that the **BCS-1** dye has a more negative HOMO energy than the  $I/I_3^-$  redox couple, leading to the regeneration of the oxidized dye. The more positive LUMO energy relative to the conduction band of  $\text{TiO}_2$  ensures an effective injection of excited electrons.

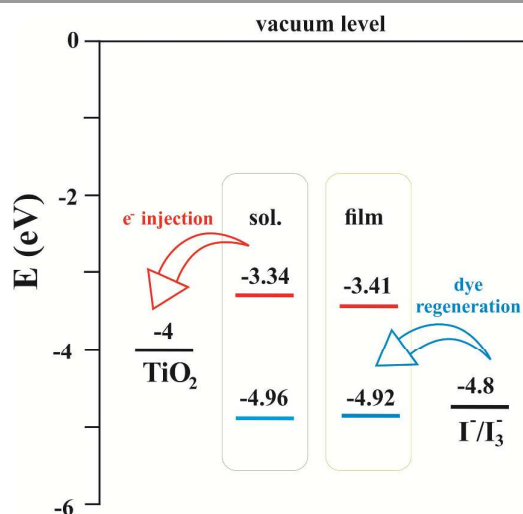
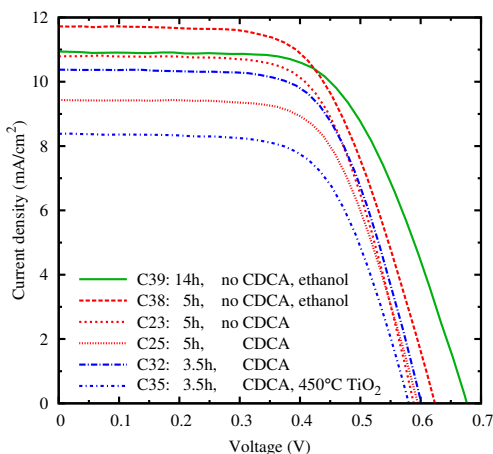


Figure 8. Band structure of BCS-1 dye vs. vacuum

### 3.5. Cell performance and discussion

The I-V characteristics of six cells, realized with and without CDCA, different functionalization time and solvents are shown in figure 9. Their complete electrical performance is presented in the table 1. Four cells (C35, C32, C25, C23) have been prepared by immersing the TiO<sub>2</sub> film in a dye solution of acetonitrile and tetrahydrofuran (6:4; v/v), while for two cells (C38 and C39), the TiO<sub>2</sub> film has been functionalized in acetonitrile:THF:ethanol (6:2:2, v/v/v). The first three cells shown in table I have been realized with CDCA in the functionalization solution.

Figure 9. I-V characteristics of six cells realized with different solvent combinations and soaking times, with and without chenodeoxycholic acid (CDCA), with (450°C) and without re-firing of the TiO<sub>2</sub> film; I-V characteristics of C38 and C39 were acquired at 0.88 Sun.

In the presence of CDCA, the increase of the functionalization time (C25 vs. C32) decreases the injected current, with a minor effect on the V<sub>OC</sub>. A similar effect was found in the absence of CDCA (C39 vs. C38), but in this case the effect on V<sub>OC</sub> is

important. Such a dependence of the efficiency on the immersion time would indicate the presence of dye aggregation<sup>44-49</sup>. Fig. 10 shows the action spectrum (IPCE, Incident Photons to Current Conversion Efficiency) of the C23 cell. The IPCE, with an onset at ≈ 650 nm and a maximum at 65 %, was recorded at 471 nm. Apparently, the 36 nm blue shift of the ICPE peak does not support the hypothesis of dye aggregation; therefore, another mechanism could be at play in degrading the open circuit voltage. A small variation of the V<sub>OC</sub> with the cheno content has been reported by Qu *et al.*<sup>50</sup> for dyes with triphenylamine moiety as donor and diketopyrrolopyrrole as core. The explanation consists in the reduction of the amount of the dye adsorbed by the coadsorbate. For dyes with triphenylamine as donor and hexyloxy chains tethered at the conjugated bridge, Chou *et al.*<sup>51</sup> found inferior efficiency when CDCA was added. This might be associated with a competition between the dye and CDCA absorption mechanisms on the TiO<sub>2</sub> surface<sup>52</sup>.

Cell	Soaking time	CDCA	J <sub>sc</sub> (mA/cm <sup>2</sup> )	V <sub>oc</sub> (V)	ff	η(%)
C35	3.5	yes	8.388	0.58	0.643	3.13%
C32	3.5	yes	10.41	0.600	0.623	3.89
C25	5	yes	9.438	0.595	0.648	3.643
C23	5	-	10.789	0.587	0.645	4.094
C38	5	-	13.647	0.625	0.603	5.14
C39	14	-	10.936	0.675	0.609	5.108

Table 1. Cells' electrical parameters

To identify the main recombination mechanism in our cells, the absolute (Mulliken) electronegativity of the dye was calculated with the formula (HOMO+LUMO)/2<sup>53,54</sup>. Using the HOMO and LUMO data of the dye in solution from the figure 8, the value of the electronegativity is -4.15eV. For the cells with V<sub>OC</sub> lower than 0.6V, the Fermi level in TiO<sub>2</sub> is estimated to be placed at about -4.2eV. Since it is slightly negative than the dye's absolute electronegativity, back electron transfer to the dye is less probable. This is a strong hint that the dominant mechanism of recombination is the electron interception by electrolyte. Therefore, keeping the electrolyte apart from the TiO<sub>2</sub> surface by increasing the concentration of the adsorbed dye would reduce the recombination with the electrolyte and, consequently, would increase V<sub>OC</sub>. However, such an effect was not observed with the TiO<sub>2</sub> functionalized in acetonitrile:THF (6:4; v/v), but it became visible when two parts of THF were replaced by ethanol. One notes that for a high performance dye (C217), Zhang *et al.*<sup>55</sup> reported a strong degradation of the efficiency when unsuitable solvent was used. The I-V characteristics of two cells prepared with TiO<sub>2</sub> immersed in acetonitrile:THF:ethanol (6:2:2; v/v/v), with the same dye concentration, no additive, but with 5 hours (C38) and 14 hours (C39) soaking time, respectively, are shown in figure 9. Both cells were measured at 0.88 Sun. For C38, both V<sub>OC</sub>=0.625V and I<sub>SC</sub>=12mA/cm<sup>2</sup> increased and the efficiency was 5.14%. The current increase can be associated with a higher dye concentration on TiO<sub>2</sub> surface, therefore a better injection, while the small V<sub>OC</sub> increase (25mV) cannot be

unequivocally attributed to the electrolyte screening by the dye scaffold on TiO<sub>2</sub> surface. That because a value of 25mV can be easily associated with a Fermi level shift toward the edge of the TiO<sub>2</sub> conduction band produced by a better electron injection into it. By contrast, for 14 hours soaking time, C39 exhibited a consistent (75mV) increase of  $V_{OC}=0.675V$  which can be associated with the inhibition of the electron interception by electrolyte. This is supported by the decrease of the short circuit current, a phenomenon attributable to dye aggregation or/and specific dye-dye<sup>56</sup> or dye-electrolyte interaction. In this respect, for a Ru-based dye, O'Regan *et al.*<sup>57</sup> reported that the electron recombination was promoted by iodide binding to the oxygen atom in a hexyloxy chain tethered at a phenyl ring. Replacing the oxygen atom by a sulphur one, the dye properties do not change but the recombination mechanism does, sulphur being a more efficient promoter than oxygen. On the contrary, Robson *et al.*<sup>58</sup> found that oxygen on the hexyloxy chain is a more efficient promoter than the sulphur. Our dye has an identical donor as C217<sup>56</sup> and one of the dyes analyzed by Robson *et al.*<sup>58</sup>, therefore a similar behaviour could be expected. In addition, it was reported<sup>59,60</sup> that the electron lifetime in a cell manufactured with a highly-conjugated triphenylamine-polyene dye, with a polarizability of 106 Å<sup>3</sup> is an order of magnitude lower than the one in a cell realized with a dye of lower polarity (46 Å<sup>3</sup>). Since calculated polarizability of our dye is 109.14 Å<sup>3</sup> (details in ESI†), a similar effect would be expected.

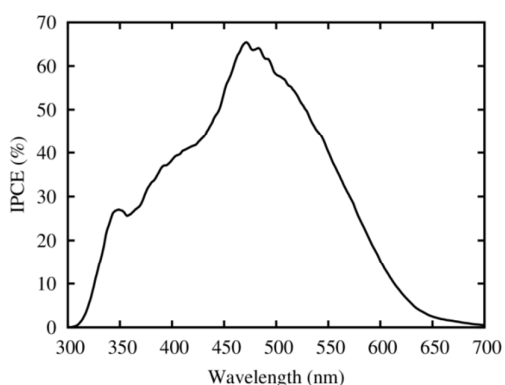


Figure 10. Incident Photons to Current Conversion Efficiency (IPCE) of C23 cell

Figure 9 also shows the I-V characteristic of a cell (C35) realized with a TiO<sub>2</sub> film re-fired at 450°C before functionalization. Both  $J_{SC}$  and  $V_{OC}$  were degraded by re-firing. To clarify the degradation mechanism, both cells realized with a 3.5h soaking time have been investigated by Electrochemical Impedance Spectroscopy (EIS)<sup>61-63</sup> and their Nyquist diagrams are presented in the figure 11. The shape of both diagrams suggests the existence of a quite strong recombination (Gerischer regime)<sup>64</sup> in both cells. However, a diagram fit using the ZSimWin 3.21 software did not give a good description with the Gerischer model, especially for the non-annealed sample (C32).

Therefore, we have used an equivalent circuit model which takes into consideration: (i) charge transfer at Pt (counter

electrode)/electrolyte interface in high frequency domain (the first semicircle from the left); (ii) the reaction at the TiO<sub>2</sub>/electrolyte interface and the electron transport in TiO<sub>2</sub> film (at intermediate frequencies, corresponding to the main semicircle observed); (iii) the ion Nernst diffusion within the electrolyte (at low frequencies, partially overlapped by the previous large semicircle when the measurements were made under illumination and absent in dark).

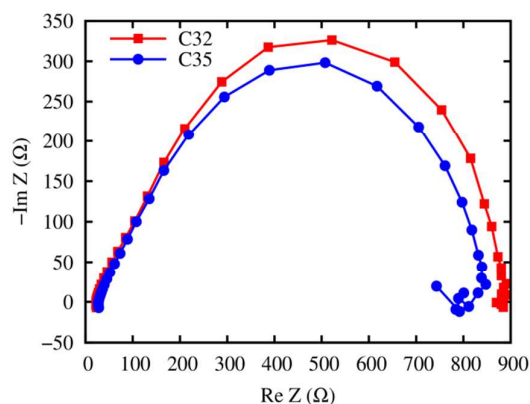


Figure 11. Nyquist diagrams of the C32 and C35 cells

Assuming for each of these interfaces a parallel resistance-capacitor group, the resulting circuit used for EIS spectra fitting is  $R_s(R_1C_1)(R_2C_2)(R_3C_3)$ . Therefore, several parameters such as series resistance ( $R_s$ ), charge transfer resistance at Pt/electrolyte interface ( $R_1$ ,  $R_{ce}$ ), charge transfer resistance at TiO<sub>2</sub>/dye/electrolyte interface ( $R_2$ ,  $R_{rec}$ ), or chemical capacitance of the TiO<sub>2</sub> film ( $C_2$ ) can be obtained from this electrochemical model. The values obtained after fitting are presented in the Table 2.

Cell no.	$R_s$	$R_1$	$C_1$	$R_2$	$C_2$	$R_3$	$C_3$
C32	8.56	10.52	6.64	253.5	41.3	41.37	19.6
C35	10.42	10.10	5.85	229.4	43.7	42.04	19.5

Table 2. Parameters obtained by fitting the experimental EIS data with a  $R_s(R_1C_1)(R_2C_2)(R_3C_3)$  equivalent circuit ( $[R] = \Omega \cdot \text{cm}^2$ ,  $[C] = \mu\text{F}/\text{cm}^2$ )

An increase in the series resistance is observed in C35 by the re-firing of the film. The resistance corresponding to the electron transfer at the counter electrode remains practically the same, indirectly indicating that the transport of the  $I_3^-$  through the TiO<sub>2</sub> pores is not affected by the film heating. The only modification appears in the value of  $R_2$ , which decreases in the case of the heated film. It points out that the charge recombination rate between the injected electrons and the acceptors from electrolyte is enhanced in the case of the heated film.

## Conclusions

A new dye comprising dihexyloxy-triphenylamine substituted moiety as donor group, furan-thiophene core as electron

## ARTICLE

## Journal Name

spacer and cyanoacrylic acid group as electron-withdrawing part has been synthesized for use in dye-sensitized solar cells. The relationship between the new push-pull dye structure and its photophysical behaviour, electrochemical properties and the performance of solar cells based on it has been thoroughly investigated. The absorption spectra are highly solvent sensitive, a strong blue shift of the main absorption maximum being registered upon solvent polarity increasing. Occurrence of the charge transfer in the excited state was evidenced by the dye photoluminescence band in the red spectral region, for DCM solution and coating. Excitation at lower wavelengths produced a splitting of the emission band in DMF solution in two peaks, indicating that the charge transfer process might be suppressed in this solvent. The electrochemical oxidation mechanism of the dye involved the formation of very stable radical cations at the triphenylamine moiety, while its cathodic reduction resulted in stable radical anions of the cyanoacrylate electron-withdrawing unit. TiO<sub>2</sub> films functionalized with various solutions of the new dye were used to test the photovoltaic cells performance. They were investigated by electrical measurements, quantum efficiency and impedance spectroscopy. The results correlate with the functionalization solution composition, functionalization time and other processes during washing and treating the film. The solar cells realized with the new sensitizer feature more than 5% efficiency, without coadsorbant and optimization. Further research will be carried out to achieve better performance. However, the nice balance of the properties encountered in this dye provides an important guideline for enlarging the selection range of building blocks for further dyes design that can be used to fabricate dye-sensitized solar cells.

## ACKNOWLEDGMENTS

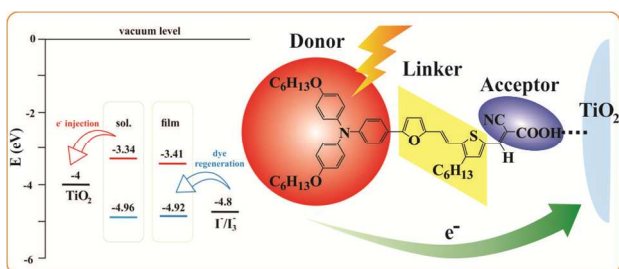
Honeywell Romania SRL acknowledges the financial support of the Romanian National Agency of Scientific Research through contract 274/2010 (European Union Structural Funds).

## References

- 1 A. Mishra, M. K. R. Fischer and P. Bäuerle, *Angew. Chem. Int. Ed.*, 2009, **48**, 2474–2499.
- 2 B. O'Regan and M. Grätzel, *Nature*, 1991, **353**, 737–740.
- 3 M. Graetzel, *Inorg. Chem.*, 2005, **44**, 6841–6851.
- 4 Y. Chiba, A. Islam, Y. Watanabe, R. Komiya, N. Koide and L. Han, *J. Appl. Phys.*, 2006, **45**, 638–640.
- 5 G. Odling, N. Chadwick, E. Frost-Pennington, D. K. Kumar, A. Ivaturi, H. M. Upadhyaya and N. Robertson, *Polyhedron*, 2015, **89**, 45–48.
- 6 B. Basheer, D. Mathew, B. K. George and C. P. R. Nair, *Solar Energy*, 2014, **108**, 479–507.
- 7 C. P. Lee, R. Y. Y. Lin, L. Y. Lin, C. T. Li, T. C. Chu, S. S. Sun, J. T. Lin and K. C. Ho, *RSC Adv.*, 2015, **5**, 23810–23825.
- 8 T. Duan, K. Fan, K. Li, W. Cao, C. Zhong, X. Chen, T. Peng and J. Qin, *Dyes Pigm.*, 2015, **117**, 108–115.
- 9 M. Matsui, N. Tanaka, Y. Ono, Y. Kubota, K. Funabiki, J. Jin, T. Inuzuka, T. Yoshida, S. Higashijima and H. Miura, *Sol. Energy Mater. Sol. Cells*, 2014, **128**, 313–319.
- 10 Z. Wan, C. Jia, Y. Duan, X. Chen, Z. Li and Y. Lin, *RSC Adv.*, 2014, **4**, 34896–34903.
- 11 L. Zhu, H. B. Yang, C. Zhong and C. M. Li, *Dyes Pigm.*, 2014, **105**, 97–104.
- 12 K. D. Seo, I. T. Choi, Y. G. Park, S. Kang, J. Y. Lee and H. K. Kim, *Dyes Pigm.*, 2012, **94**, 469–474.
- 13 C. Zhong, J. Gao, Y. Cui, T. Li and L. Han, *J. Power Sources*, 2015, **273**, 831–838.
- 14 A. Venkateswararao, K. R. Justin Thomas, C. T. Li and K. C. Ho, *RSC Adv.*, 2015, **5**, 17953–17966.
- 15 K. S. V. Gupta, J. Zhang, G. Marotta, M. A. Reddy, S. P. Singh, A. Islam, L. Han, F. de Angelis, M. Chandrasekharan and M. Pastore, *Dyes Pigm.*, 2015, **113**, 536–545.
- 16 J. Liu, X. Yang, J. Zhao and L. Sun, *RSC Adv.*, 2013, **3**, 15734–15743.
- 17 Z. J. Ning and H. Tian, *Chem. Commun.*, 2009, **45**, 5483–5495.
- 18 W. Wu, J. Yang, J. Hua, J. Tang, L. Zhang, Y. Long and H. J. Tian, *Mater. Chem.*, 2010, **20**, 1772–1779.
- 19 R. Li, X. Lv, D. Shi, D. Zhou, Y. Cheng, G. Zhang and P. Wang, *J. Phys. Chem. C*, 2009, **113**, 7469–7479.
- 20 *EU Pat.*, 13180787.7-1555, 2013.
- 21 H. Yamanishi, I. Tomita, K. Ohta and T. Endo, *Mol. Cryst. Liq. Cryst.* 2001, **169**, 47–61.
- 22 C. Wang and L. R. Dalton, *Tetrahedron Lett.*, 2000, **41**, 617–620.
- 23 A. D. Becke, *J. Chem. Phys.*, 1993, **98**, 5648–5652.
- 24 C. Lee, W. Yang and R. G. Parr, *Phys. Rev. B*, 1988, **37**, 785–789.
- 25 R. Krishnan, J. S. Binkley, R. Seeger and J. A. Pople, *J. Chem. Phys.*, 1980, **72**, 650–654.
- 26 A. D. McLean and G. S. Chandler, *J. Chem. Phys.*, 1980, **72**, 5639–5648.
- 27 T. Clark, J. Chandrasekhar, G. W. Spitznagel and P. von Ragué Schleyer, *J. Comp. Chem.*, 1983, **4**, 294–301.
- 28 C. J. Cramer, in *Essentials of computational chemistry: Theories and models*, John Wiley & Sons, Chichester, 2nd edn., 2005.
- 29 T. Yanai, D. Tew and N. Handy, *Chem. Phys. Lett.*, 2004, **393**, 51–57.
- 30 I. Ciofini, T. le Bahers, C. Adamo, F. Odobel and D. Jacquemin, *J. Phys. Chem. C*, 2012, **116**, 11946–11955.
- 31 C. Adamo and D. Jacquemin, *Chem. Soc. Rev.*, 2013, **42**, 845–856.
- 32 M. J. Frisch, G. W. Trucks, H. B. Schlegel, G. E. Scuseria, M. A. Robb, J. R. Cheeseman, G. Scalmani, V. Barone, B. Mennucci, G. A. Petersson, H. Nakatsuji, M. Caricato, X. Li, H. P. Hratchian, A. F. Izmaylov, J. Bloino, G. Zheng, J. L. Sonnenberg, M. Hada, M. Ehara, K. Toyota, R. Fukuda, J. Hasegawa, M. Ishida, T. Nakajima, Y. Honda, O. Kitao, H. Nakai, T. Vreven, J. A. Montgomery, J. E. Peralta, F. Ogliaro, M. Bearpark, J. J. Heyd, E. Brothers, K. N. Kudin, V. N. Staroverov, R. Kobayashi, J. Normand, K. Raghavachari, A. Rendell, J. C. Burant, S. S. Iyengar, J. Tomasi, M. Cossi, N. Rega, J. M. Millam, M. Klene, J. E. Knox, J. B. Cross, V. Bakken, C. Adamo, J. Jaramillo, R. Gomperts, R. E. Stratmann, O. Yazyev, A. J. Austin, R. Cammi, C. Pomelli, J. W. Ochterski, R. L. Martin, K. Morokuma, V. G. Zakrzewski, G. A. Voth, P. Salvador, J. J. Dannenberg, S. Dapprich, A. D. Daniels, Ö. Farkas, J. B. Foresman, J. V. Ortiz, J. Cioslowski and D. J. Fox, in *Gaussian 09 Revision D.01*, Gaussian Inc., Wallingford, 2013.
- 33 R. Dennington, T. Keith and J. Millam, in *Gaussview Version 5*, Semichem Inc., Shawnee Mission, 2009.
- 34 S. Paek, H. Choi, H. Choi, C. W. Lee, M. Kang, K. Song, M. K. Nazeeruddin and J. Ko, *J. Phys. Chem. C*, 2010, **114**, 14646–14653.
- 35 S. Amthor, B. Noller and C. Lambert, *Chem. Phys.*, 2005, **316**, 141–152.
- 36 J. Salbeck, U. Schöberl, K. M. Rapp and J. Daub, *J. Phys. Chem.*, 1991, **171**, 191–212.

- 37 T. Ivan, L. Vacareanu and M. Grigoras, *ISRN Organic Chemistry*, 2012, Article ID 976178.
- 38 M. D. Damaceanu, H. D. Gilsing, B. Schulz, A. Arvinte, M. Bruma, *RSC Adv.*, 2014, **4**, 52467-52475.
- 39 A. B. Nepomnyashchii and B. A. Parkinson, *ACS Appl. Mater. Interfaces*, 2014, **6**, 14881–14885.
- 40 Y. Takeda, T. L. Andrew, J. M. Lobe, A. J. Mork and T. M. Swager, *Angew. Chem.*, 2012, **124**, 9176–9180.
- 41 A. Tigreros, V. Dhas, A. Ortiz, B. Insuasty, N. Martín and L. Echegoyen, *Sol. Energy Mater. Sol. Cells*, 2014, **121**, 61–68.
- 42 A. Hagfeldt and M. Graetzel, *Chem. Rev.*, 1995, **95**, 49–68.
- 43 J. B. Asbury, Y. Q. Wang, E. Hao, H. N. Ghosh and T. Lian, *Res. Chem. Intermed.*, 2001, **27**, 393–406.
- 44 A. Kay, R. Humphry-Baker and M. Graetzel, *J. Phys. Chem.*, 1994, **98**, 952–959.
- 45 K. Hara, Y. Danoh, C. Kasada, Y. Ohga, A. Shinpo, S. Suga, K. Sayama and H. Arakawa, *Langmuir*, 2004, **20**, 4205–4210.
- 46 R. Caballero, E. M. Barea, F. Fabregat-Santiago, P. de la Cruz, L. Márquez, F. Langa, J. Bisquert, *J. Phys. Chem. C*, 2008, **112**, 18623–18627.
- 47 Z. S. Wang, N. Koumura, Y. Cui, M. Takahashi, H. Sekiguchi, A. Mori, T. Kubo, A. Furube, K. Hara, *Chem. Mater.*, 2008, **20**, 3993–4003.
- 48 K. Kalyanasundaram and M. Gratzel, *Coord. Chem. Rev.*, 1998, **177**, 347–414.
- 49 B. O'Regan, L. Xiaoe and T. Ghaddar, *Energy Environ. Sci.*, 2012, **5**, 7203–7215.
- 50 S. Qu, W. Wu, J. Hua, C. Kong, Y. Long and H. Tian, *J. Phys. Chem. C*, 2010, **114**, 1343–1349.
- 51 H. H. Chou, Y. C. Chen, H. J. Huang, T. H. Lee, J. T. Lin, C. Tsai and K. Chen, *J. Mater. Chem.*, 2012, **22**, 10929–10938.
- 52 S. P. Singh, M. S. Roy, K. R. J. Thomas, S. Balaiah, K. Bhanuprakash and G. D. Sharma, *J. Phys. Chem. C*, 2012, **116**, 5941–5950.
- 53 R. S. Mulliken, *J. Chem. Phys.*, 1934, **2**, 782–793.
- 54 R. G. Parr and R. G. Pearson, *J. Am. Chem. Soc.*, 1983, **105**, 7512–7516.
- 55 G. Zhang, H. Bala, Y. Cheng, D. Shi, X. Lv, Q. Yu and P. Wang, *Chem. Commun.*, 2009, **16**, 2198–2200.
- 56 E. M. Barea and J. Bisquert, *Langmuir*, 2013, **29**, 8773–8781.
- 57 B. C. O'Regan, K. Walley, M. Juozapavicius, A. Anderson, F. Matar, T. Ghaddar, S. M. Zakeeruddin, C. Klein and J. R. Durrant, *J. Am. Chem. Soc.*, 2009, **131**, 3541–3548.
- 58 K. C. D. Robson, K. Hu, G. J. Meyer and C. P. Berlinguette, *J. Am. Chem. Soc.*, 2013, **135**, 1961–1971.
- 59 M. Miyashita, K. Sunahara, T. Nishikawa, Y. Uemura, N. Koumura, K. Hara, A. Mori, T. Abe, E. Suzuki and S. Mori, *J. Am. Chem. Soc.*, 2008, **130**, 17874–17881.
- 60 T. Marinado, K. Nonomura, J. Nissfolk, M. K. Karlsson, D. P. Hagberg, L. Sun, S. Mori and A. Hagfeldt, *Langmuir*, 2010, **26**, 2592–2598.
- 61 J. Bisquert, *J. Phys. Chem. B*, 2002, **106**, 325–333.
- 62 F. Fabregat-Santiago, G. Garcia-Belmonte, I. Mora-Sero and J. Bisquert, *Phys. Chem. Chem. Phys.*, 2011, **13**, 9083–9118.
- 63 Q. Wang, S. Ito, M. Grätzel, F. Fabregat-Santiago, I. Mora-Seró, J. Bisquert, T. Bessho and H. Imai, *J. Phys. Chem. B*, 2006, **110**, 25210–25221.
- 64 J. Bisquert, I. Mora-Sero and F. Fabregat-Santiago, *ChemElectroChem*, 2014, **1**, 289–296.

## Table of contents



A new D- $\pi$ -A dye based on dihexyloxy-substituted triphenylamine moiety has been synthesized and its preliminary performances in DSSCs are reported.